Applied Energy 342 (2023) 121158

Contents lists available at ScienceDirect

Applied Energy

journal homepage: www.elsevier.com/locate/apenergy

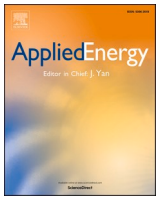

Solidification performance improvement of phase change materials for latent heat thermal energy storage using novel branch-structured fins and nanoparticles

Ji Zhang [a], Zhi Cao [a], Sheng Huang [a], Xiaohui Huang [a], Yu Han [b,*], Chuang Wen [c,*], Jens Honoré Walther [d], Yan Yang [c,*]

[a] School of Electrical and Information Engineering, Hunan University, Changsha 300072, China
[b] School of Mechanical and Electrical Engineering, Suqian University, Suqian 223800, China
[c] Faculty of Environment, Science and Economy, University of Exeter, Exeter, EX4 4QF, UK
[d] Department of Civil and Mechanical Engineering, Technical University of Denmark, DK-2800 Kgs. Lyngby, Denmark

HIGHLIGHTS

- Combination of branch-structured fins and nanoparticles to enhance PCM discharging performance.
- Quantitative assessment of parametric studies in improving the PCM solidification performance.
- 5% volume fractions of nanoparticles reduce 9.3% solidification time of PCMs.
- The combination of the fins-nanoparticle idea reduces the discharging time by 85%

ARTICLE INFO

Keywords:
Energy storage
Solidification
Nanoparticle
Branch-structured fin
Phase change material
Heat transfer enhancement

ABSTRACT

In the present study, we propose the combination of novel branch-structured fins and Al_2O_3 nanoparticles to enhance the performance of a phase change material (PCM) during the solidification process in a triple-tube heat exchanger. The inevitable drawback of PCMs is their lower heat conductivity, which can result in a long response time during the phase change process in latent heat thermal storage systems. Therefore, any serious improvement strategy needs an optimized phase change process. A mathematical model for a two-dimensional structure composed of a PCM with paraffin RT82 and Al_2O_3 nanoparticles that considers the thermal conduction in metal fins, Brownian motion of nanoparticles, and natural convection in a liquid phase PCM is proposed and verified based on experimental results. The impact of various volume fractions and fin layouts on the solidification process is discussed, involving the evolution and deformation of solid–liquid interfaces and distribution of isotherms and average temperature and liquid fraction curves. The results imply that the solidification behaviour can be significantly enhanced by the application of nanoparticles and metal fins. Compared with the inherent structure of the heat exchanger, the solidification time is decreased by 8.5%, 9.3%, and 10.3% for Al_2O_3 nanoparticles (at 2%, 5%, and 8%, respectively) only and by 83.0%, 80.7%, 80.8%, and 82.9%, respectively, for various fin layouts only. This is attributed to increased heat transfer by thermal conduction and natural convection. It can be concluded that the impact of the use of fins is preferable compared to that for nanoparticles, and the benefit of nanoparticles is limited.

1. Introduction

The need to reduce the emissions from burning fossil fuels and focus on global warming and resource limitation impacts is a growing concern worldwide. In this regard, the presently applied environmentally friendly resources, such as solar, wind, hydropower, etc., have been extensively developed as a relatively effective solution [1]. However, the natural characteristic of intermittency restricts further application,

* Corresponding authors.
E-mail addresses: yuhan.neu@gmail.com (Y. Han), c.wen@exeter.ac.uk (C. Wen), yanyang2021@outlook.com, y.yang7@exeter.ac.uk (Y. Yang).

https://doi.org/10.1016/j.apenergy.2023.121158
Received 15 December 2022; Received in revised form 24 March 2023; Accepted 15 April 2023

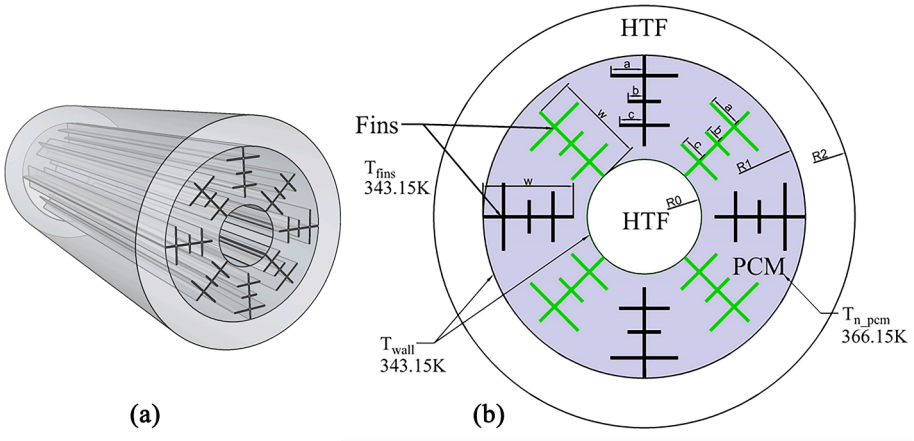

Fig. 1. The triplex-tube thermal storage system configurations with fins: (a) a three-dimensional physical model and (b) a two-dimensional cross-section domain: black fins are bonded to the outer tube and green fins are bonded to the inner tube.

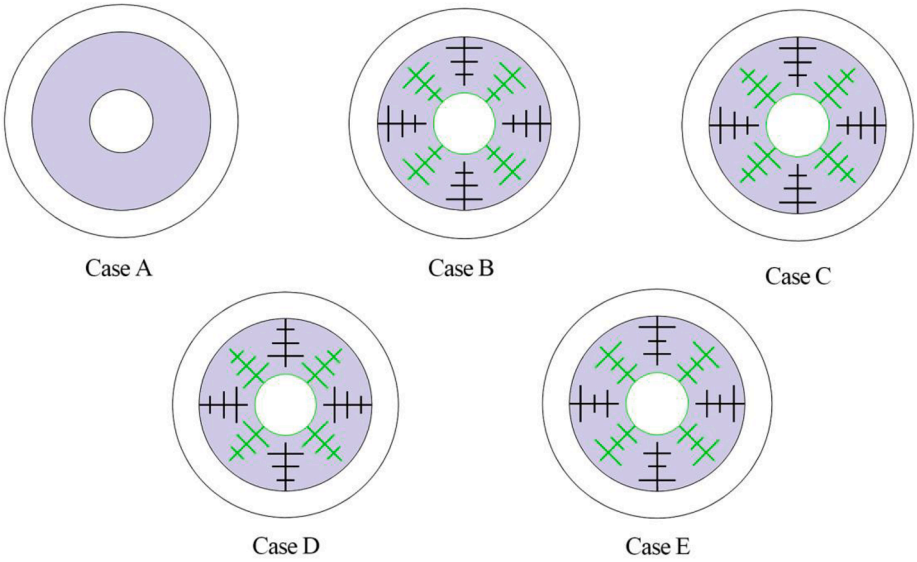

Fig. 2. The cross-section configurations in various fin layouts.

resulting in less competition for these resources in the energy markets. Therefore, the use of a thermal energy storage system as a supplementary part is regarded as an attractive method. The purpose of employing this system is to store heat energy to balance the existing break between the energy requirement and supply. There are three choices available: a sensible heat strategy based on varying the temperature of storage materials, a latent heat strategy based on a phase change process for storage materials, and a chemical strategy based on chemical reactions for energy storage. Based on phase change materials (PCMs), the latent heat energy storage method has been studied by numerous researchers on account of its excellent capacity to restore large amounts of energy with only a small temperature change, high latent heat of fusion for PCMs and nearly isothermal nature save course compared with the sensible heat storage strategy [2]. However, the cost of producing PCMs is one of the primary drawbacks. This may generate high expenses when PCMs are distributed to real industry applications, i.e., heating and cooling systems, and energy storage systems. One of the solutions is to use cheaper materials with additional new techniques to improve their performance. For example, general paraffin could be used as a medium for energy storage by using fins or nanoparticles to improve their thermal conductivities.

The low thermal conductivity of PCMs results in a long response time for the charging/discharging process. This can impact the rate of energy storage and recovery; hence, enhancement methods need to be combined to improve heat transfer. A wide range of heat transfer enhancement methods has been reported such as those based on the use of metal fins [3,4], heat pipes [5], metal foams [6], nanoparticles [7,8], and multitubes [9]. Among these methods, metal fins are a commonly used enhancement method between PCMs and heat transfer fluids (HTFs) in various fin configuration structures, such as circular, longitudinal, rectangular, etc. The use of these structures is highly attractive due to the features of economic cost, ease of manufacture, and good adaptability. Liu et al. [10] numerically studied a shell and tube latent heat thermal storage device employing a longitudinal triangular fin structure. They analyzed the dynamic temperature response, effects of the fin geometric parameters, fin materials, and initial temperature during the solidifying process for three different fin structures. The results showed that the use of longitudinal triangular fins can lead to an enhancement of the solidification performance. The solidifying time was improved by applying materials with high thermal conductivity and increasing the fin lengths or decreasing the initial temperature. It was found that the temperature difference between the PCM and internal wall should be over 20 K to achieve a relatively faster cooling rate. Huang et al. [11] numerically investigated the solidifying performance in a finned shell

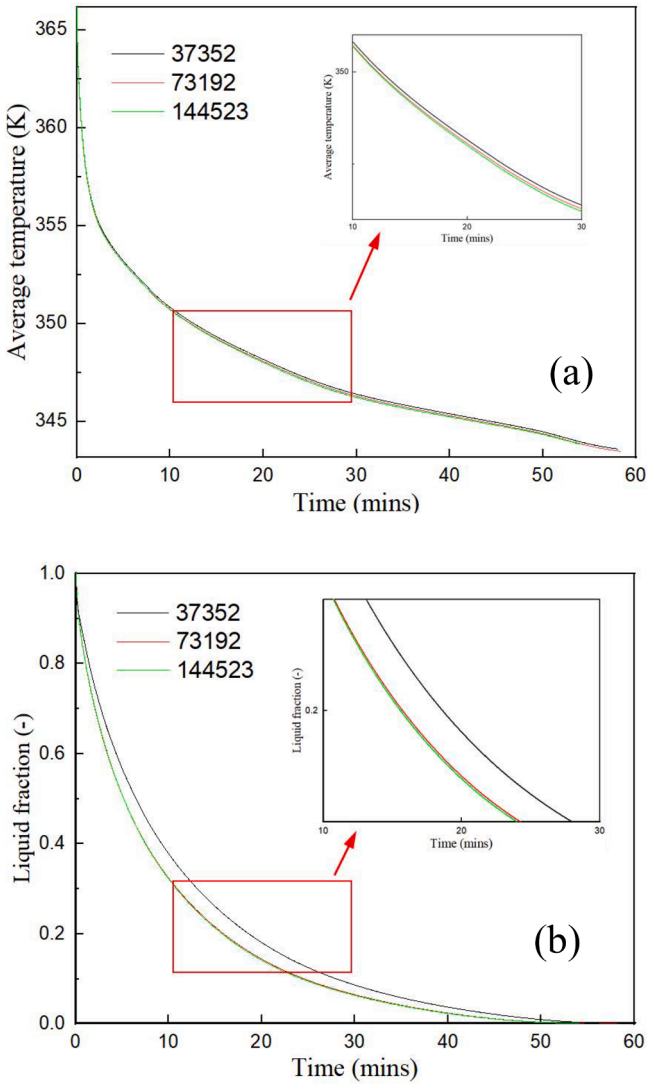

Fig. 3. Grid independency analysis: (a) average temperature and (b) liquid fraction.

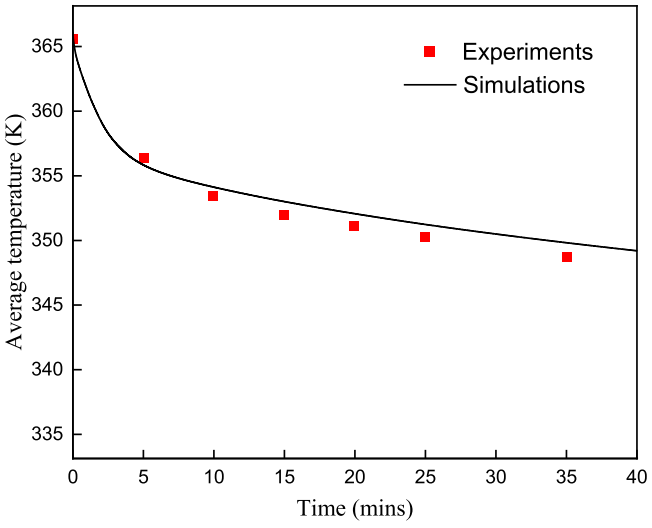

Fig. 4. Comparison of the temperature data obtained from simulation and experiment from Al-Abidi et al. [23].

and tube ice storage apparatus compared with that for the same unit without fins, and the discharging response and ice front evolution were analyzed as well. They chose structural parameters such as fin thickness, length, and numbers to investigate the impact of the solidification process. The results imply that natural convection is bad for solidification behaviour and that the application of fins can enhance the energy-discharging process because of the coupling effect of thermal conduction enhancement and natural convection suppression. They also found that the fin thickness and number can significantly influence the storage performance. Wu et al. [12] numerically studied the solidification efficiency of spiderweb-like fins compared with plate fins structures under the same volume and revealed a solidification strengthening mechanism and the role of natural convection. The results imply that the heat transmission hysteresis zone is eliminated because of the application of spiderweb-like fins and that the entire solidifying time for new structure fins is shortened by 47.9%. In addition, although the heat transmission of the solidification course is dominated by natural convection at the early stages, thermal conduction dominates in the later stages. Patel et al. [13] studied the performance of both solidifying and melting rates for PCMs considering longitudinal fins with three different parameters, such as fin shape, fin number and arrangement. They developed a melting/solidifying model based on two dimensions for PCMs, and the results indicate that an arrangement with eight fins is the most effective for the combined melting-solidification duration, and the enhancement of performance due to an increase in the number of fins with a reduced length is significant.

Generally, employing fins as a kind of enhancement method is an efficient way to improve heat transfer, while combining fins with nanoparticles as another commonly used method can be used to further improve the charging/discharging process. This is because of the better heat storage behaviour and higher heat conductivity of nanoparticles. Researchers have reported corresponding studies for different nanoparticles coupled with fins in various structures. Sheikholeslami et al. [14] numerically studied the heat transfer performance of nanoparticles (Cu) during the solidifying process through an enclosure with V-shaped fins. The effect factors, such as the concentration and size of nanoparticles, length of fins, and angle of V-shaped fins, were considered. The consequences reveal that the solidification rate is increased with an increase in the angle of the V-shaped fin and that the augmentation of the fin length can lead to a decreased solidification rate. Mahdi et al. [15] numerically investigated the simultaneous charging-discharging process for an energy storage system with various fin configurations and nanoparticles (Al_3O_2) in a triplex-tube heat exchanger (TTHX) applying paraffin as a PCM. To obtain the optimal fin configuration, a response surface methodology (RSM) considering different fin geometric parameters is employed. The results indicate that the optimal fin structure proposed in the triplex-tube heat exchanger is preferable compared with the usage of nanoparticles in the same volume. Hosseinzadeh et al. [16] studied the solidifying process using PCM with fins and Al_2O_3 – Go hybrid nanoparticles as enhanced technology in a latent heat thermal energy storage system. The effect of adding fins and nanoparticles is analyzed, and fins with different thicknesses were also investigated. In addition, the response surface method (RSM) is applied to find the best fin configuration for the system. They demonstrated that the use of an optimal fin structure can lead to a higher solid fraction rate compared with only dispersing hybrid nanoparticles in the PCM. Qin et al. [17] numerically studied the freezing process in an annulus zone using paraffin as the PCM and Al_2O_3 nanoparticles as an enhanced strategy. The governing parameters included the sizes and positions of the fins as well as the volume fraction of the nanoparticles. The results imply that the solidifying rate is increased by approximately 14.5% by varying the position of the fins.

Alizadeh et al. [18] studied the solidification course employing nanoparticles combined with V-shaped fins as enhanced strategies for PCMs in a triple-tube latent heat thermal energy storage system that aims to balance the energy supply and requirement. In addition, they

Table 1
The relative error between experimental and numerical results.

Experiment (K)	365.61	356.38	353.49	352.03	351.14	350.29	348.77
Simulation (K)	366.15	355.84	354.13	353.01	352.08	351.24	349.81
Error (%)	0.15	0.15	0.18	0.28	0.27	0.27	0.30

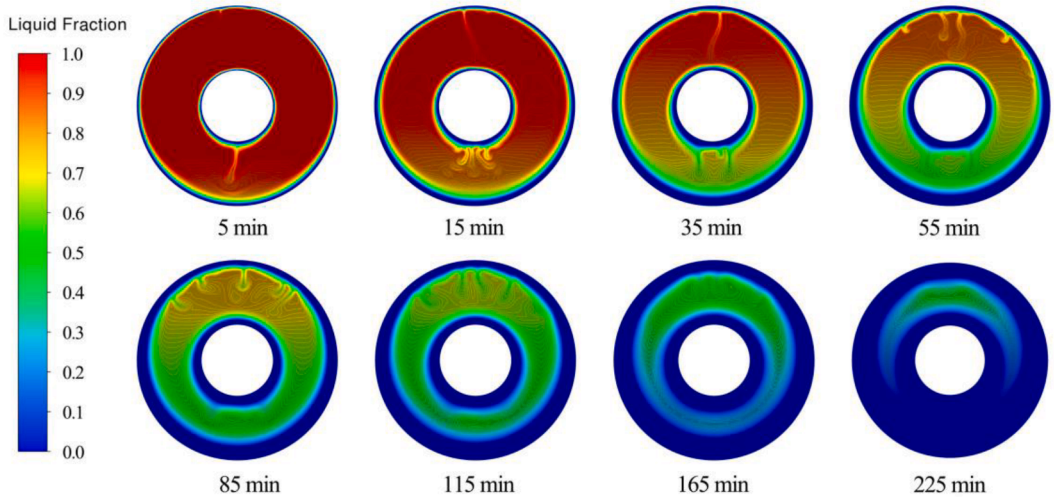

Fig. 5. The contours for the solidifying liquid fraction of phase change materials for Case A.

applied the response surface method (RSM) to optimize the parameters of the system. The results show that the application of a V-shaped fin in the system leads to a higher solidification rate in comparison with nanoparticle dispersion in different volume fractions. Sarani et al. [19] used nanoparticles with a distribution of discontinuous strip fins as a solution to the long response time problem in PCM energy storage systems. The researchers chose the fin materials and the distribution of fins as effect factors to find the optimal structure. The results indicate that the application of discontinuous fins can lead to an obvious enhancement of the response time and that the application of nanoparticles contributes little to improving the discharging time. Mahdi et al. [20] numerically investigated the influence of incorporating Al_2O_3 on the solidification process of a PCM (RT82) in a triplex-tube heat exchanger (TTHX). The heat transfer characteristics and impacts of incorporating nanoparticles over different stages were analyzed. The results indicate that a nanoparticle concentration in the range of 3–8% can save the completed solidification time between 8% and 20%, whereas at the early stages of the solidification course, the presence of nanoparticles makes little difference. Elbahjaoui et al. [21] employed a numerical method to research the melting behaviour of a PCM (paraffin wax) with Al_2O_3 nanoparticles in the rectangular latent heat storage part. They considered the Reynolds number and Rayleigh number of the flow characteristics, the thermal performance of the storage unit, the volumetric fraction of the nanoparticles, and the effect of the aspect ratio. The results indicate that the dispersion of high-conductivity nanoparticles can lead to a decrease in the melting time with augmentation in the volume fraction of nanoparticles ($\leq$8%). In addition, an increased Rayleigh number can influence the melting time to improve energy storage in the form of sensible heat.

The objective of this paper is to numerically investigate the heat transfer improvement during the solidification process employing fins combined with Al_2O_3 nanoparticles in a triplex-tube heat exchanger. The TTHX is selected because of its large heat transfer area and the annulus space that can house PCM with nanoparticles. A two-dimensional computational fluid dynamics model is proposed that considers the thermal conduction and natural convection in fins and the Brownian motion of nanoparticles. The various volume fractions of Al_2O_3 nanoparticles as enhancement methods in the original structure are studied, and the impact of different positions of longitudinal fins with three different lengths on the solidifying process for the PCM is discussed. Based on the fin length, we develop four diverse fin layouts to determine the optimal structure for which the solidification rate is significantly improved. In addition, the variation in the solid–liquid interfaces and the average temperature in the heat exchanger employing the aforementioned fin layouts are investigated, and the different enhanced strategies are compared based on the average temperature and liquid fraction curves.

The knowledge gap that this work can fill includes a) How does the combination of fins and nanoparticles affect the solidification process of PCMs for energy storage performance? b) What is the role of nanoparticles in enhancing the discharging process of PCMs compared to the branch-structured fins? and c) The quantitative analysis of parametric studies of fins and nanoparticles in improving the PCM solidification performance. The qualitative and quantitative evaluations in the present study are useful to improve the understanding of discharging performance of PCMs in thermal energy storage units.

2. Problem descriptions

Fig. 1 shows the schematic diagram of a finned triplex-tube heat exchanger for (a) a three-dimensional physical model and (b) a two-dimensional cross-section model with boundary and initial conditions. TTHX is widely employed in the beverage, food and medical pharmaceutical industries and has a larger thermal-exchanger area compared with the double-tube heat exchanger [22]. Additionally, it can be used to make the phase change process faster, leading to a decreased response time. Al-Abidi et al. [23] used a triplex-tube heat exchanger as a thermal energy storage unit with PCM in a solar-powered liquid desiccant air conditioning system. As shown in Fig. 1(b), the original structure only includes three concentric tubes that are made of copper, while fins, represented by black and green colours are incorporated with the internal and external tubes in the paper to improve the heat transfer. Three different lengths of external and internal longitudinal fins are selected. The use of higher thermal conductivity copper tubes enhances the heat

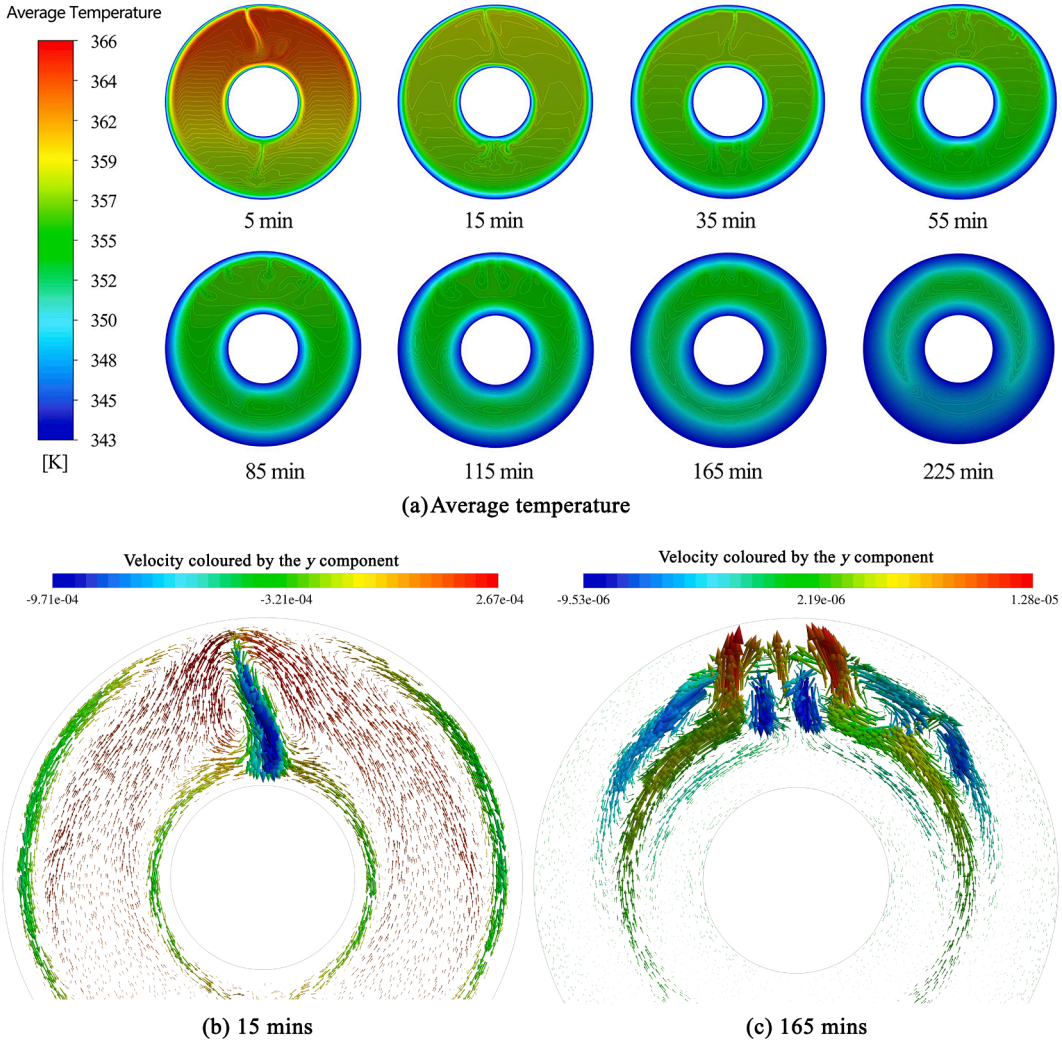

Fig. 6. Isotherm and vectors for the solidifying process of the PCM for Case A.

transmission between the PCM and HTF. The computational domain represented by the shadow areas is PCM or PCM with nanoparticles, and the blank sections are filled with HTF for the TTHX. While the overall length of the heat exchanger is 500 mm, the inner, middle, and outer tubes have radii of 26.6, 75, and 100 mm with thicknesses of 1.2, 2, and 2 mm, respectively. Eight fins that are oriented perpendicular to the walls have thicknesses and lengths (w) of 1 mm and 42 mm, and the parameters a, b and c represent different longitudinal lengths. In addition, the cross-section plot of the original TTHX and four different fin layouts proposed in the paper for Cases A to E are illustrated in Fig. 2. The related arguments in cases for various fin layouts across the annulus are listed in a previous paper [24]. Considering the material cost and space for installation, the 90° interval for the fins incorporated in the inner and middle tubes is chosen to ensure uniform heat transmission. Alumina (Al_2O_3) is employed as nanoparticles, paraffin (RT82) is chosen as the PCM due to its long lifetime and excellent stability without the supercooling effect, and water is chosen as the HTF on account of its high heat capacity and ease of preparation.

Initially ($t = 0$), the temperature of the walls and fins is set as 343.15 K (same as the HTF), and the temperature of the PCM with nanoparticles or PCM is set to 366.15 K. The solidification temperature of the PCM is 350.15 K due to the liquidus temperature of the PCM being 358.15 K, the PCM is regarded as a liquid, and the boundary condition is sufficiently low to maintain the solidification process. For time $t > 0$, the PCM in the heat exchanger will form a temperature gradient at this moment, meaning that natural convection and thermal conduction are affected simultaneously. As the temperature gradient forms, the direction of heat transfer is outward, and each surface will start to appear in the solidified layer.

3. Governing equations and numerical model

While the PCM flow is solidifying, both conduction and convection will play an important role in the solid and liquid phases. The conservation equations of continuity, momentum and energy employed to numerically describe the temperature distribution and fluid motion are defined as follows [28-30]:

$$\nabla \bullet \mathrm{U} = 0 \tag{1}$$

$$\frac{\partial u}{\partial t} + U \bullet \nabla u = \frac{1}{\rho}\left(-\nabla p + \mu \nabla^2 u\right) + C\frac{(1-\gamma)^2 u}{\gamma^3 + \varepsilon} \tag{2}$$

$$\frac{\partial v}{\partial t} + U \bullet \nabla v = \frac{1}{\rho}\left(-\nabla p + \mu \nabla^2 v + \rho\beta g\left(T - T_{ref}\right)\right) + C\frac{(1-\gamma)^2 v}{\gamma^3 + \varepsilon} \tag{3}$$

$$\frac{\partial h}{\partial t} + \frac{\partial(\Delta H)}{\partial t} + \nabla \bullet (Uh) = \nabla \bullet \left(\frac{k}{\rho C_p}\nabla H\right) \tag{4}$$

where $U = (u, v)^T$. As the PCM with nanoparticles solidifies, a constant C is defined to describe the mushy zone state and how fast it reduces to

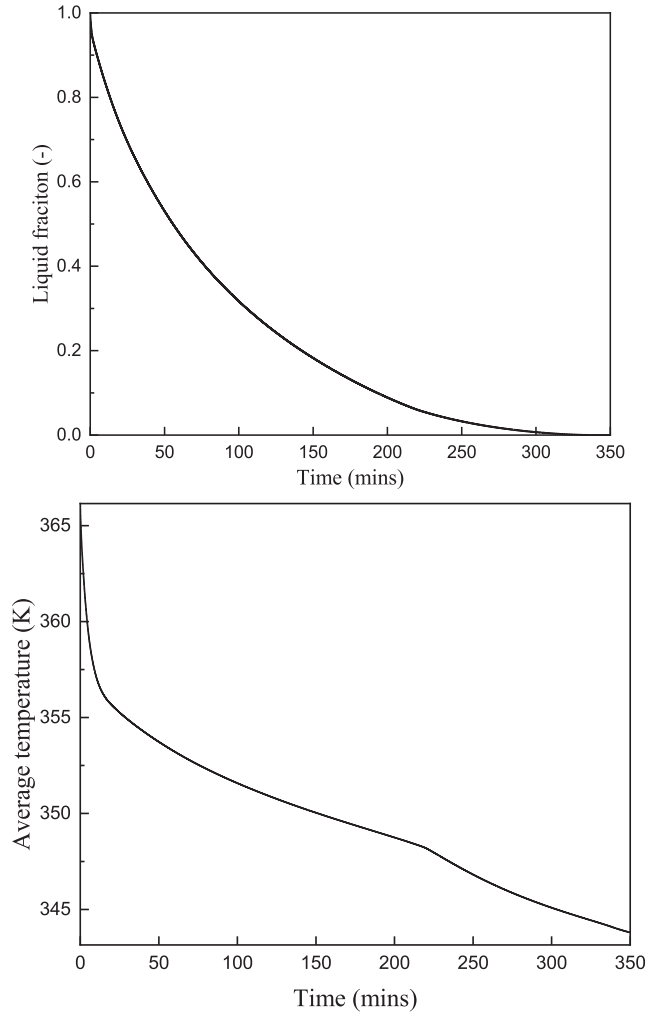

Fig. 7. The average temperature and liquid fraction curves for Case A.

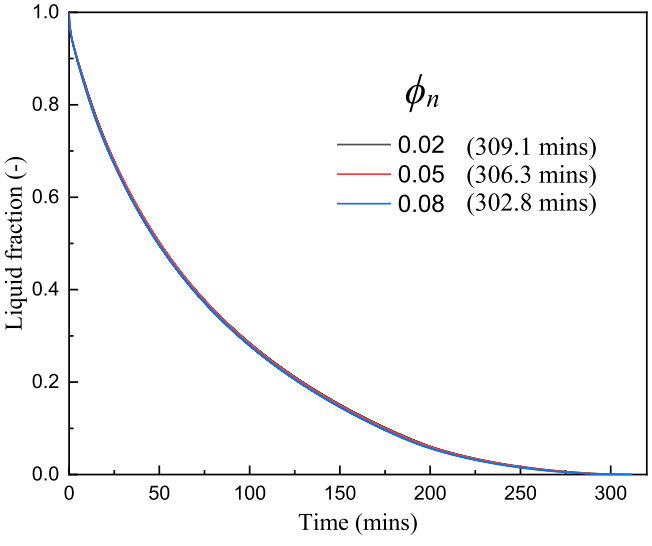

Fig. 8. The various concentrations of Al_2O_3 in the liquid fraction for the original structure.

zero. Generally, this constant is set to a number ranging from 10^5-10^6 for many studies [31]. For the present study, the constant $C = 10^5$ was found to produce results in good agreement with experimental data of Al-Abidi et al. [23]. In addition, to avoid division by zero, a small constant ($\varepsilon = 0.001$) is defined, and ΔH represents the latent heat. h represents the sensible enthalpy, which is expressed as follows [32-34]:

$$h = h_{ref} + \int_{T_{ref}}^{T} C_p dT \tag{5}$$

where the relevant enthalpy can be calculated using

$$H = h + \Delta H \tag{6}$$

$$\Delta H = \gamma L \tag{7}$$

where L is the latent heat of fusion, γ represents the varying liquid fraction as the PCM solidifies between temperature T_s and T_l, which is defined as [35-37]:

$$\gamma = \begin{cases} 0, & T \leqslant T_s \\ \dfrac{(T - T_s)}{(T_l - T_s)}, & T_s < T < T_l \\ 1, & T_l \leq T \end{cases} \tag{8}$$

In addition, to investigate the temperature field in the fins, the corresponding governing energy equation can be expressed as [28]:

$$\frac{\partial\left(\rho_f C_{p_f} T_f\right)}{\partial t} = \nabla \bullet \left(k_f \nabla T_f\right) \tag{9}$$

The parameters in this equation are dependent on the fin material. To further improve heat transmission, dispersion nanoparticles are commonly used during the solidification process. The thermophysical properties can be found in Ref [8]. To vary the corresponding parameters, such as the volume fraction (ϕ_n) of PCM with nanoparticles, the following equations are used [24]:

$$\rho_{n_{pcm}} = \phi_n \rho_n + (1 - \phi_n)\rho_{pcm} \tag{10}$$

$$\left(\rho C_p\right)_{n_{pcm}} = \phi_n \left(\rho C_p\right)_n + (1 - \phi_n)\left(\rho C_p\right)_{pcm} \tag{11}$$

$$(\rho L)_{n_{pcm}} = (1 - \phi_n)(\rho L)_{pcm} \tag{12}$$

$$(\rho\beta)_{n_{pcm}} = \phi_n (\rho\beta)_n + (1 - \phi_n)(\rho\beta)_{pcm} \tag{13}$$

$$\mu_{n_{pcm}} = 0.983 e^{(12.959\phi_n)} \mu_{pcm} \tag{14}$$

$$k_{n_{pcm}} = \frac{k_n + 2k_{pcm} - 2\left(k_{pcm} - k_n\right)\phi_n}{k_n + 2k_{pcm} + \left(k_{pcm} - k_n\right)\phi_n} k_{pcm} + 5 \times 10^4 \beta \vartheta \phi_n \rho_{pcm} C_{p_{pcm}} \sqrt{\frac{k_B T}{\rho_n d_n}} f(T, \phi_n) \tag{15}$$

$$f(T, \phi_n) = \left(2.8217 \times 10^{-2}\phi_n + 3.917 \times 10^{-3}\right)\frac{T}{T_{ref}} + \left(-3.0669 \times 10^{-2}\phi_n - 3.91123 \times 10^{-3}\right) \tag{16}$$

where k_B is the Boltzmann constant, β is the thermal expansion coefficient calculated using $\beta_{Al_2O_3} = 8.4407(100\phi_n)^{-1.07304}$ with concentration ranging from $1\% \leq \phi_n \leq 10\%$ and temperature region of $298K \leq T \leq 363K$ [38], and $f(T, \phi_n)$ is a function. In addition, it is worth noting that the equations include the impact of Brownian motion (second part in Eq. (15)) on the temperature dependence, size and concentration of the alumina nanoparticles. Because no Brownian motion occurs in the solid phase of the PCM, ϑ is used as a correction factor to describe the state.

A numerical model of the PCM with nanoparticles is developed using enthalpy-porosity methodology. The mushy zone as a region that exists in the solid and liquid phases is modelled as a "pseudo" porous medium

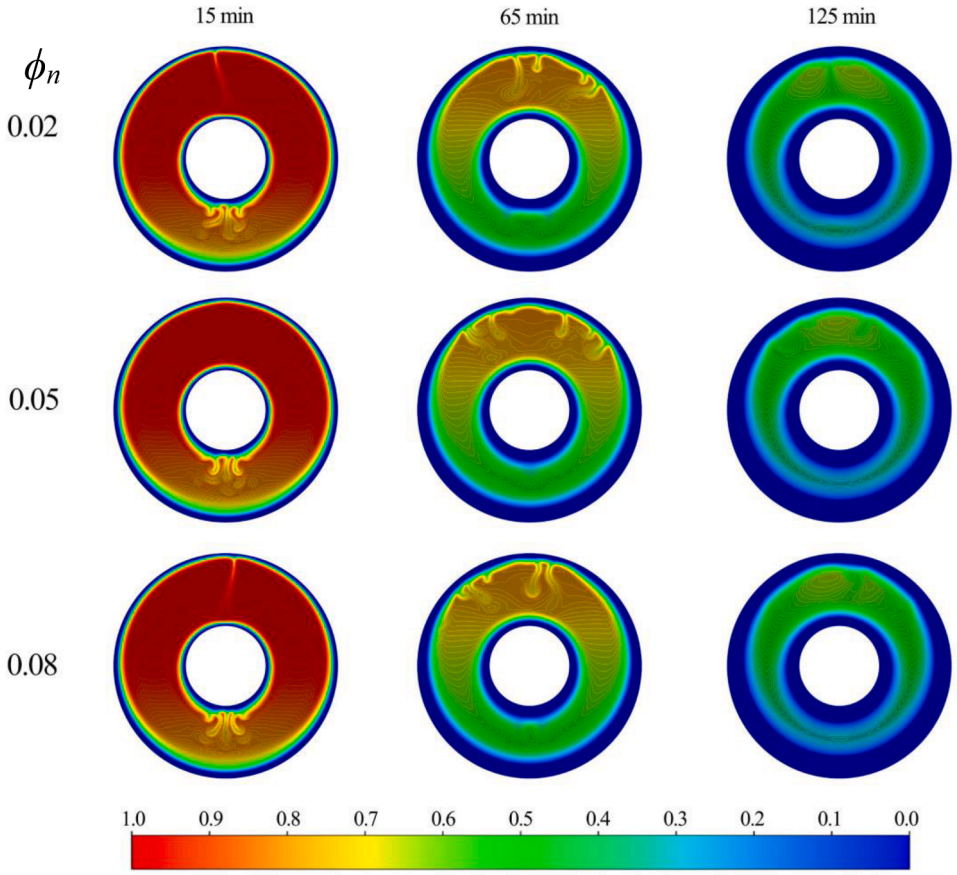

Fig. 9. Liquid fraction contour graphs for various concentrations of nanoparticles for Case A.

with a porosity decreasing from 1 (liquid) to 0 (solid) when the materials are solidified [25]. To define the physical properties of the PCM and various concentrations of nanoparticles, a number of user-defined functions (UDFs) based on C++ language are used. The UDFs are loaded into the Fluent solver to solve the energy and momentum equations. In addition, since the heat exchanger is stationary and the solidification course proceeds simultaneously, the use of a two-dimensional model can be considered to be proper, and the computational time cost is another vital influencing factor. For details on the application of FLUENT, the solver type is chosen using the pressure-based method with absolute velocity formulation under a transient time type, and the acceleration due to gravity is taken to be $-9.81\ m/s^2$ in the Y direction. The governing equations are discretized by the finite volume method and the semi-implicit method for the pressure-linked equations (SIMPLE) algorithm is employed for the calculation of the pressure–velocity coupling [26]. The PRESTO scheme is applied for the correction of the pressure equation [27]. The second-order upwind is chosen for the spatial discretization of energy and momentum, and the first-order implicit option is chosen for the transient formulation. The time-step is 0.1 s to ensure that the solution is stable, and the under-relaxation factors for energy, velocity components, and pressure correction are set as 1, 0.5 and 0.3, respectively. The condition of pre-determined convergence for continuity and momentum equations is 10^{-4}, and that for the energy equation is 10^{-6}.

4. Results and discussion

4.1. Verification

4.1.1. Grid independence analysis

The grid independency is analyzed for three different numbers of cells 37352, 73192, and 144523, with Case E of Fig. 2 selected as the computational layout. The variation in the average temperature and liquid fraction curves for a diverse number of grids is shown in Fig. 3. It can be observed that the differences are decreased with the augmentation of the grid numbers. In addition, to ensure that the results are stable, the time step is set as 0.1 s, and a cell number of 73,192 is selected for the grid for the computational case to describe the accuracy. A further increase in the cell number for the grid led to little change in the average temperature and liquid fraction curves, and the computational time cost is considered as well.

4.1.2. Validation of the numerical model

The numerical model proposed in this paper employs a previous study by Al-Abidi et al. [23] to verify identical initial and boundary conditions and related experimental data. The simulation data are compared with the experimental data obtained for the solidifying performance of paraffin (RT82) with nanoparticles (Al_2O_3) in the annulus of a triple-tube heat exchanger (TTHX). A comparison of the average temperature obtained from the two studies during solidification is shown in Fig. 4. It can be observed that while the results of the simulation are in an acceptable range although they do not fully capture the experimental data. Table 1 is used to further clarify the accuracy of the model. It can be seen that the maximum relative error between experimental measurements and numerical results is around 0.30%. This demonstrates that our developed model is accurate to describe the solidification process of phase change materials.

4.2. Solidifying process of the inherent structure

The solidification course in the triple-tube heat exchanger is elucidated by none-enhanced strategies (Case A) of Fig. 2 for the distribution

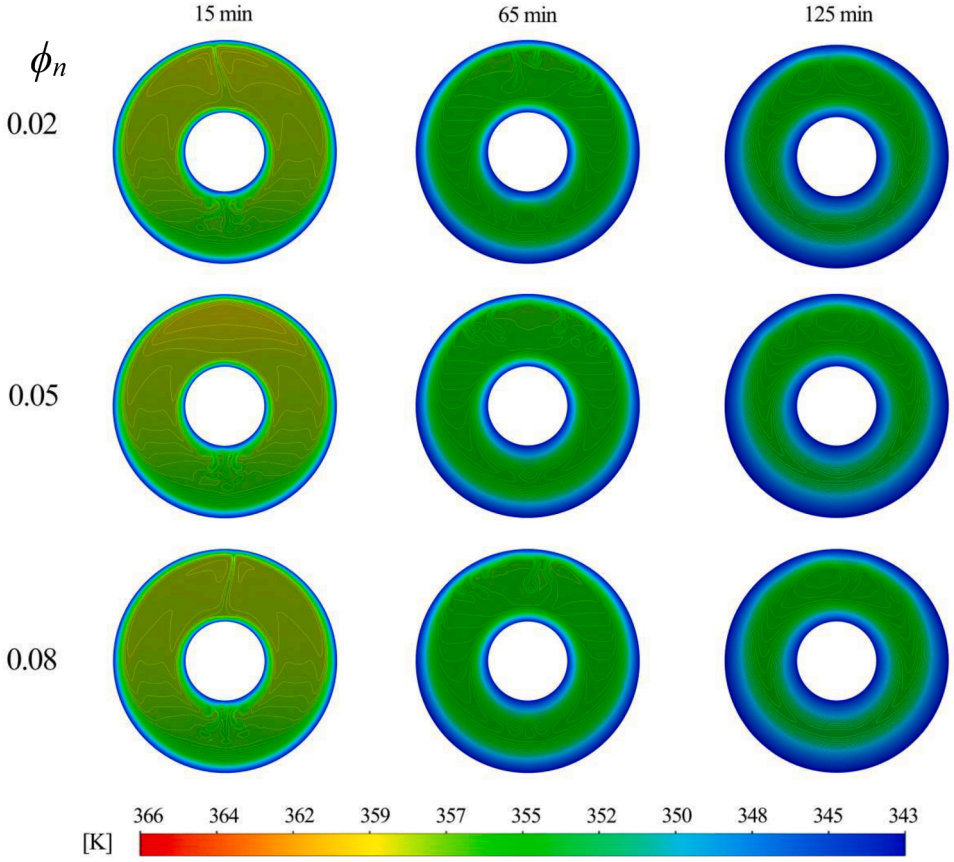

Fig. 10. Distribution of isotherms for various concentrations (ϕ_n) of nanoparticles for Case A.

of temperatures and varying solid–liquid interfaces. The whole solidifying time is 337.6 min under the initial temperature conditions. The different periods of liquid-fraction contours at certain intervals are shown in Fig. 5. Fig. 6 shows the evolution of the isotherms while Fig. 7 represent the variations in the profiles of the average temperature and liquid fraction.

As shown in Fig. 5, the blue and red areas represent the solid and liquid phases, respectively, and the light green colour represents the solid–liquid interfaces. The temperature differences influence the intensity of the thermal conduction and natural convection that occurs during the whole process of PCM solidification. At the initial time of 5 mins, it can be observed that two solidified layers are formed with independent solid–liquid interfaces, and the direction of deformation is oriented toward the annulus. Due to the effect of gravity, the solidifying process proceeds at the downward region of the annulus first, which means that the heat transfer is dominated by natural convection. At 15 min, the deformation of solid–liquid interfaces begins to form adjacent to the annulus, and some raised sections form. This is because of a change in the density of the paraffin, and a loss of fluidity for the liquid phase PCM is apparent. With time, at 35 min, the solid–liquid interface of the internal part continues to expand and tends to be smooth. Below the tube, due to the effect of buoyancy and variation in paraffin density, the solidifying speed starts to decrease, and the role of natural convection is restricted. As solidification proceeds, at 55 min, it can be observed that the amount of liquid phase for the upper half of the sample is decreased, and the shape of the solid–liquid interface exhibits different irregular parts. This is due to the impact of the temperature drop on the interaction between thermal conduction and natural convection. In addition, further shrinkage of the solid–liquid interfaces signifies that heat transfer continuously proceeds. At 85 min, the main difference in this period is the decline in the overall liquid fraction, and for the downward area of the solid–liquid interface, which is more uniform, the internal layer expands continually. As the solidifying process continues, at 115 min, the thermal conduction dominates the heat transfer, and the increase in the solid phase paraffin content retards the Brownian motion. At the half section of the heat exchanger, the solid–liquid interfaces substantially shrink, and the liquid fraction of the overall solid phase continues to decrease. With time, at 165 min, due to the augmentation of PCM density and the effect of gravity, the size of the underlying solid–liquid interfaces continues to shrink, and the upper part starts to merge. The temperature of the solid phase is close to the wall temperature, so the time required for the solidifying process is increased. At 225 min, while the maximal temperature of the PCM is close to the wall temperature, the upper part of the tube still contains unsolidified sections.

The distribution of temperature plots for the original structure investigated in the paper is presented in Fig. 6 over eight periods of time. For the solidifying course, the temperature change is continuous and dynamic; at the same time, the temperature gradient directly influences heat transmission. For the initial time, the impact of thermal conduction and natural convection will reach a maximum extent due to the maximal temperature difference between the PCM and wall. The isotherms fill the overall space across the heat exchanger because the liquid phase of the PCM is dominant. Due to the effect of gravity, the temperature of the upper half of the annulus is higher than that of the downward part, and two concentric circles close to the wall are formed to represent the solid–liquid interface. At 15 min, some small vortices are formed in the downward part of the internal tube due to the buoyancy force that originates from the variation in density between the cold and hot liquids. The solid–liquid interfaces develop toward the annulus. With time, at 35 min, compared to the preceding period, the main difference is the disappearance of vortices due to a weakening of natural convection and an increase in the amount of solid phase. At 55 min, the shape of the solid–liquid interfaces at the upper part of the heat exchanger is significantly deformed, but the colour does not change much. At 85 min,

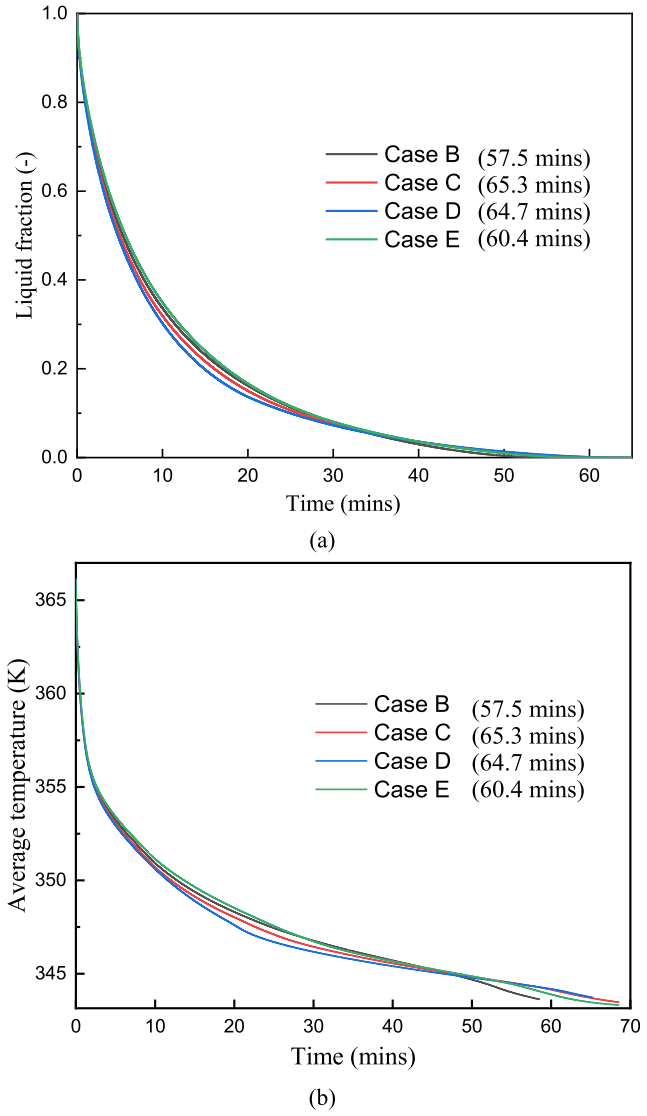

Fig. 11. (a) The liquid fraction and (b) temperature curves for various fin structures.

the solid–liquid interfaces near the internal wall develop more smoothly, and the upper vortices start to decrease. At this moment, the free natural convection stops being effective, and the heat transmission is dominated by thermal conduction. With time, at 115 min, the rate of increase in the solid phase content close to the internal and external walls continues to increase. At 165 min, the solidifying speed for the downward area is much higher due to the impact density, and the vortices at the upper part of the tube merge. At 225 min, the solid–liquid interface at the downward area in the annulus nearly disappears, which means that the solidifying process is close to completion, and convection has only a small impact.

4.3. Enhancement methods for nanoparticles

Nanoparticles, as one of the enhancement strategies, are generally employed because of their modification of both viscosity and thermal conductivity. In this study, the impact of the concentration and dispersion of Al_2O_3 nanoparticles in a heat exchanger with volume fractions of 2%, 5%, and 8% are analysed. In addition, a new correction for the heat conductivity of Al_2O_3 nanoparticles based on a test developed by Vajjha et al. [29] is employed, which is shown in Eq. (15), for a $\beta_{Al_2O_3}$ concentration in the range of $1\% \leq \phi_n \leq 10\%$. The results obtained for different concentrations of nanoparticles in the liquid fraction curve are shown in Fig. 8. As shown in the figure, the differences among the various concentrations are small, but the enhancement methods that involve employing nanoparticles can lead to a reduction in the solidification time by 8.5%, 9.3%, and 10.3% compared to the original structure (with a complete solidification time of 337.6 mins which is not shown in Fig. 8).

Fig. 9 shows the contours at 15 min, 65 min, and 125 min in three different volume fractions. In this figure, at 15 min, due to natural convection across the annulus of the heat exchanger being more obvious, the vortices are first formed at the lower part. The deformation of solid–liquid interfaces for three volume fractions is distinguished near the internal wall, and the augmentation of the volume fraction can increase the area of the vortices. Compared with the original fin layout (Case A in which there are no fins shown in Fig. 2), the rate of deformation for the nanoparticle case develops slightly faster due to the dispersion of nanoparticles presenting a higher convection contribution. With time, at 65 min, deformation of the solid–liquid interface is found to occur in the upper part of the annulus, as the effect of natural convection as a useful heat transmission mode starts to weaken during the solidification process. With the presence of nanoparticles, the thermal resistance against heat transfer is increased. With increasing time, at 125 min, the differences in the density of the liquid PCM are significant, and due to the weak buoyancy effect, the solidification process in the upper area is slower than that in the downward area. With respect to the dispersion of nanoparticles, there is little influence on the deformation of the solid–liquid interfaces with increasing nanoparticle volume fraction.

The distribution of temperature at various periods is shown in Fig. 10. From this figure, among the various volume fractions, there is no noticeable impact of the isotherms across the heat exchanger. This is why the improvement in the solidification time due to the use of nanoparticles is limited. On the one hand, the dispersion of nanoparticles can only further enhance thermal conduction because of the higher heat conductivity and viscosity between the walls and liquid PCM. On the other hand, the augment of the nanoparticle can limit the role of natural convection so that a modest improvement in the solidifying speed of the phase change course is obtained.

4.4. Solidifying process for novel branch-structured fins

In this section, metal fins are applied to the enhanced solidifying process in the TTHX. Based on a previous study by Al-Abidi et al. [23], four different fins layouts are proposed to investigate the solidification performance. To study on the impact of the fins, Fig. 11 shows the average temperature and liquid fraction curves obtained for different cases, Fig. 12 represents the contour plots for the liquid fraction over various periods, and the variation in the isotherm plots over the various periods is shown in Fig. 13.

Fig. 11(a) represents the solidifying rate of the liquid fraction in different cases. As shown in this figure, the full solidifying time is 57.51 min for Case B, 65.32 min for Case C, 64.75 min for Case D, and 60.45 min for Case E. The proposal of novel fins' structures can decrease the solidifying time by 83.0%, 80.7%, 80.8%, and 82.9%, respectively, compared with the inherent structure of a triplex-tube heat exchanger. Therefore, the application of fins leads to a significant improvement in the solidifying course on account of an enhancement of the heat transfer intensity. The differences among these cases expressed from 5 min to 30 min are apparent due to the impact of heat conduction and natural convection, but the solidifying time for the whole process in different cases is small. In addition, Fig. 11(b) describes the evolution of the average temperature for the various cases, and it can be seen that the data show a difference mainly from 10 min to 40 min.

4.4.1. The evolution of the solid–liquid interfaces

Fig. 12 represents the evolution of the solid–liquid interfaces for

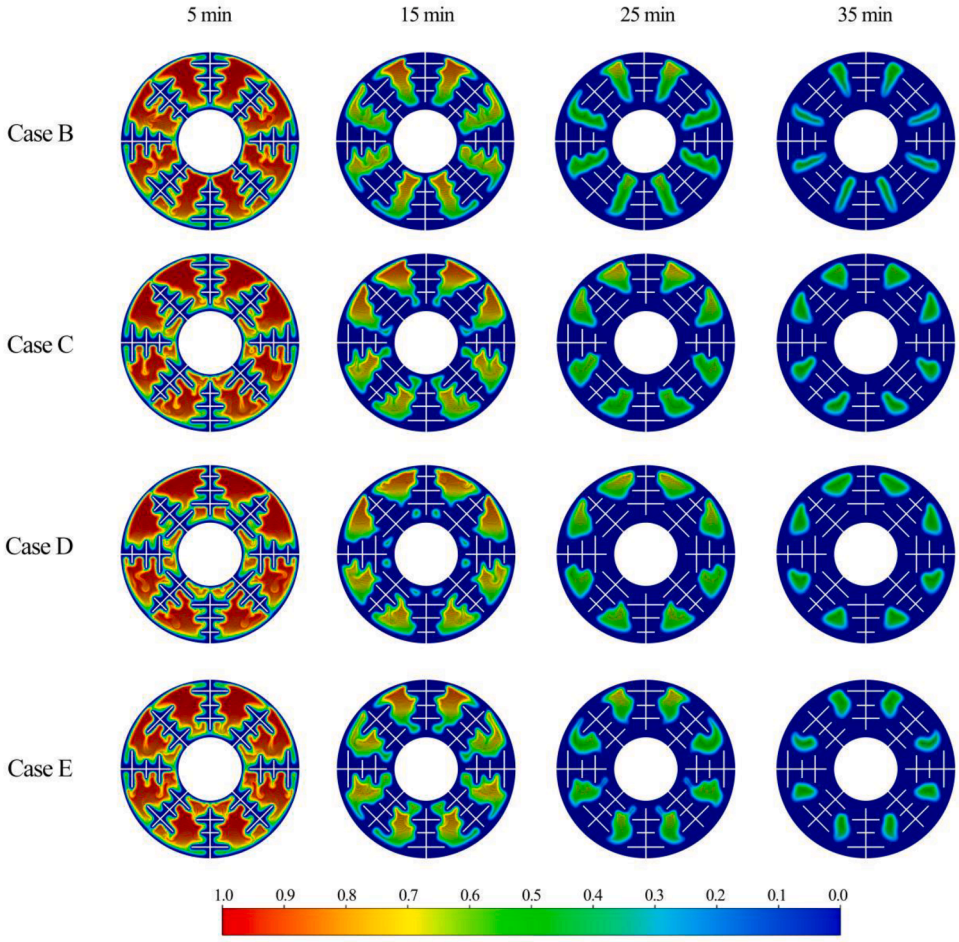

Fig. 12. The variation in the solid–liquid interfaces (liquid fraction).

various fin layouts. In this figure, four time periods of 5 min, 15 min, 25 min and 35 min are chosen to describe the solidifying process. At 5 min, all cases form significant solid–liquid interfaces because of the temperature difference between the PCM and walls, which influences the intensity of natural convection and heat conduction. The application of fins increases the contact area between the PCM and cold boundaries, and due to the relatively higher thermal conductivity of copper, the solidifying process is enhanced. Although the lengths of the fins in various cases lead to no differences, the fin position directly influences the space of the PCM in the annulus.

In addition, it can be observed that a significant solid area is formed near the fins, which means that the fins can well promote heat transfer, and the evolution of solid–liquid interfaces at the downward part in the annulus is faster than the upper part because of the variation in the PCM density so that the liquid phase area appears to be distributed. At 15 min, it can be observed that while the colour of the annulus is similar, the deformation of solid–liquid interfaces shows a significant variation due to the attenuation of natural convection and augmentation of density in the liquid phase. During this period, as the liquidity of the liquid phase declines, thermal conduction plays a crucial role in the solidifying course. The fin layout results in various shapes of solid–liquid interface parts, and the length of the fins are directly relevant to the thermal resistance for the heat transfer. In addition, as shown in the figure, the areas of the solid–liquid interfaces near the longer fins have a relatively smaller proportion. This is because longer fins can benefit from the transfer of heat directly to the PCM in the evolution of the solidification course across the annulus. As the solidifying process continues, at 25 min, from Case B to E, the solid–liquid interfaces shrink significantly, and because of the impact of density and gravity, the solidifying rate in the downward part of the annulus is faster than that in the upper part. The shape of the solid–liquid interface is spotted except for Case B, which is banded, and the liquid fraction (represented by the colour) is lower than that in the past period. At this point, the central area near the internal wall is already solidified in all cases. At 35 min, most of the areas across the annulus for the solid phase have already formed, and the solid–liquid interface continues to shrink. Although the colours observed for all cases are comparable, the shape of the solid–liquid interface for Case B is slender. That is why the solidifying process for Case B is the fastest, and it can be concluded that the increase in the length of the fins with tube radius can result in a good solidifying speed in the course of heat transfer across the annulus.

4.4.2. Analysis of the isotherm plots

The distributions of the isotherm plots for various fin layouts are shown in Fig. 13. The heat transmission for natural convection and thermal conduction can directly influence the shape change of solid–liquid interfaces and the speed of the solidification process. At 5 min, as shown in the graph, the solid phases of PCM are formed near and around the fins due to the direct heat transport pathway provided by the fins. The fin layout determines the shapes of solid–liquid interfaces, and the temperature difference between PCM and walls can lead to the achievement of increased heat transfer during this period. With time, at 15 min, although the shapes of the structures for the solid–liquid interface are different, they are found to gather at the fin intervals and shrink. This is due to the buoyancy force generated by the density difference impacting the intensity of the natural convection. As the

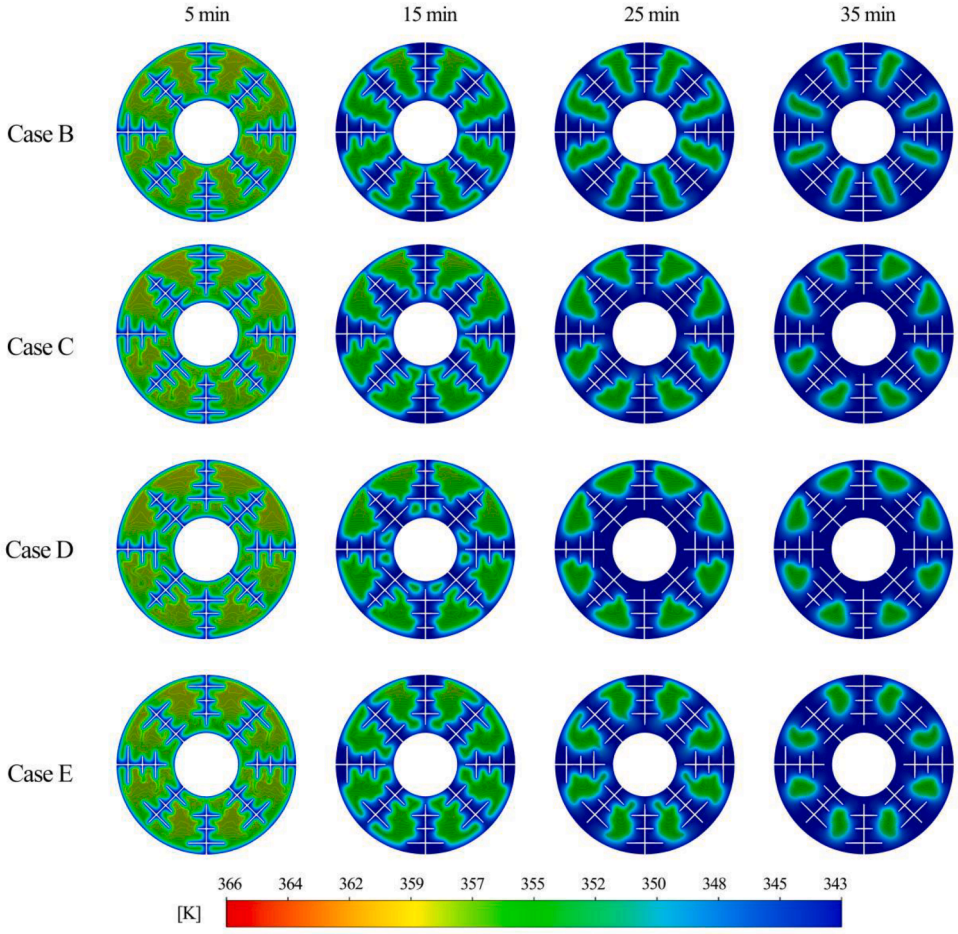

Fig. 13. The distribution of the isotherms.

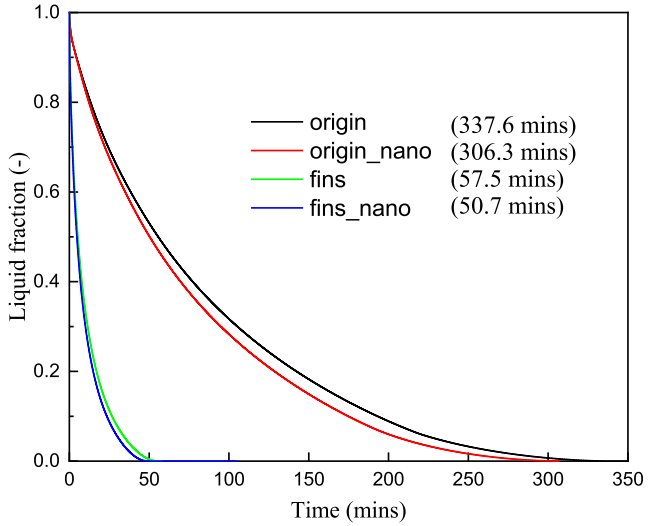

Fig. 14. The liquid fraction curves obtained for the different enhancement methods.

solidifying process proceeds, at 25 min, from Case C to E, the internal part of the PCM in the liquid phase transforms into the solid phase. The solid–liquid interfaces for all cases further shrink, and the effect of natural convection decreases significantly. This is because applying the fins results in a more intense augmentation of density in the PCM and thermal conduction in the solid phase. At 35 min, the isotherms for all cases show the same colour due to the overall space in the approximately equal temperature, and then the thermal transfer is dominated by heat conduction. Natural convection has little effect due to the areas of the solid phase already formed.

4.5. Comparison of all enhanced strategies

Fig. 14 shows the solidifying speed for various enhanced methods based on the liquid fraction curves. In this figure, four kinds of cases are chosen: origin structure, origin with 5% nanoparticles, the optimal fin layout and fins with 5% nanoparticles, respectively, at four periods of solidification: 10, 20, 30 and 40 min. The complete solidification times are 337.6 min (origin structure without fins and nanoparticles), 306.3 min (origin with nanoparticles but no fins), 57.5 min (fins only) and 50.7 min (fins with nanoparticles). Compared with the original structure of the triple-tube heat exchanger, the application of enhanced methods can lead to a reduction in the solidifying time of 9.3%, 83.0%, and 85.0%, respectively. Therefore, it can be concluded that fins can be used to improve the solidification process. Compared with nanoparticles, the extent of the enhanced solidifying rate of the fins has great advantages.

To better investigate the solidifying process, Fig. 15 shows a comparison of the contour plots obtained for the different enhancement strategies studied in this paper. As shown in the figure, the differences between the origin structure (without fins and nanoparticles) and origin with nanoparticles are concentrated on the downward section of the internal wall and the upper section of the external wall. This is because of the impact of natural convection, which is expressed as buoyancy dominating at the initial time. For the cases with fins, the shape

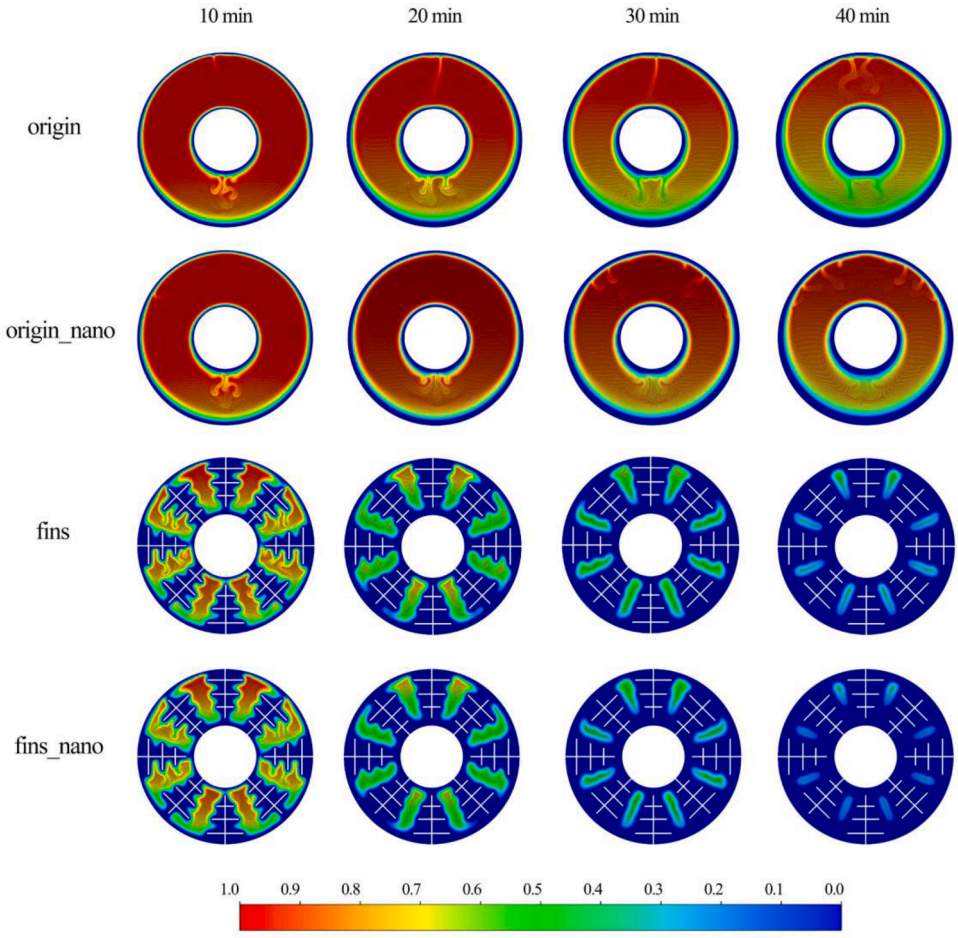

Fig. 15. A comparison of the contour plots for different cases.

variation of the solid–liquid interfaces for fins with nanoparticles is relatively smaller than that for the fin-only case, which means that the use of nanoparticles can lead to an improvement in the solidifying process but with a limited effect. In addition, compared to the no-fin cases, solid–liquid interfaces for the with-fin cases show significant variation.

5. Conclusions

The solidification process for heat transmission in a triple-tube heat exchanger (TTHX) with enhancement methods, such as nanoparticles and metal fins, used to increase the solidification speed is studied numerically in this paper. Based on a two-dimensional mathematical model, the solidification process for the original structure without any improvement strategies is addressed and discussed first. Three fins of various lengths are formed with or without Al_2O_3 nanoparticles at different concentrations in four kinds of layouts, which are then used to study variations in the liquid fraction and temperature for enhancing the solidification process. Meanwhile, the distribution of isotherms and variation in the solid–liquid interfaces across a heat exchanger for PCMs with nanoparticles are discussed. The consequences reveal that the application of fins and nanoparticles has a significant effect on the discharging rate during the solidification process.

The heat transfer for natural convection and thermal conduction directly influences the process of solidification. Compared with the original structure without fins and nanoparticles, the usage of nanoparticles can only reduce the solidification time by 8.5%, 9.3%, and 10.3% using 2%, 5% and 8% volume fractions, respectively. In addition, the application of fins in different layouts can reduce the solidification time by 83.0%, 80.7%, 80.8%, and 82.9%, respectively. This demonstrates that the use of metal fins offers a much better enhancement method than that based on the use of nanoparticles. Longer fins located near the external wall contribute more to the solidification process. Natural convection plays an important role initially, while thermal conduction influences heat transfer during the entire process. This is because of the augmentation of PCM density and the limitation of flow generated by the fin structure.

It is realized that the effect of the nanoparticles is evaluated based on the assumptions that the nanoparticles are distributed uniformly in the PCM. This assumption limits the understanding of the effect of nanoparticles on the solidification process of PCMs at the molecular level, which needs to be clarified in future studies. Also, parametric optimization will be carried out in the future to achieve better performance of the PCM solidification including the length of fins, number of fins, and different materials of nanoparticles.

CRediT authorship contribution statement

Ji Zhang: Investigation, Discussion, Writing - Original draft preparation and Revising. **Zhi Cao:** Investigation, Writing - Original draft preparation and Revising. **Sheng Huang:** Discussion and Reviewing. **Xiaohui Huang:** Discussion and Reviewing. **Yu Han:** Conceptualization, Methodology, Investigation, Reviewing and Revising. **Chuang Wen:** Conceptualization, Supervision, Discussion, Reviewing and Revising. **Jens Honoré Walther:** Discussion, Reviewing and Revising. **Yan Yang:** Supervision, Conceptualization, Methodology, Discussion, Reviewing and Revising

Declaration of Competing Interest

The authors declare that they have no known competing financial interests or personal relationships that could have appeared to influence the work reported in this paper.

Data availability

Data will be made available on request.

References

[1] Al-Maghalseh M, Mahkamov K. Methods of heat transfer intensification in PCM thermal storage systems: review paper. Renew Sustain Energy Rev 2018;92:62–94. https://doi.org/10.1016/j.rser.2018.04.064.

[2] Tao YB, Liu YK, He YL. Effects of PCM arrangement and natural convection on charging and discharging performance of shell-and-tube LHS unit. Int J Heat Mass Transf 2017;115:99–107. https://doi.org/10.1016/j.ijheatmasstransfer.2017.07.098.

[3] Huang X, Yao S. Solidification performance of new trapezoidal longitudinal fins in latent heat thermal energy storage. Case Stud Therm Eng 2021;26:101110. https://doi.org/10.1016/j.csite.2021.101110.

[4] Ji C, Qin Z, Dubey S, Choo FH, Duan F. Simulation on PCM melting enhancement with double-fin length arrangements in a rectangular enclosure induced by natural convection. Int J Heat Mass Transf 2018;127:255–65. https://doi.org/10.1016/j.ijheatmasstransfer.2018.07.118.

[5] Motahar S, Khodabandeh R. Experimental study on the melting and solidification of a phase change material enhanced by heat pipe. Int Commun Heat Mass Transf 2016;73:1–6. https://doi.org/10.1016/j.icheatmasstransfer.2016.02.012.

[6] Mahdi JM, Nsofor EC. Multiple-segment metal foam application in the shell-and-tube PCM thermal energy storage system. J Energy Storage 2018;20:529–41. https://doi.org/10.1016/j.est.2018.09.021.

[7] Sheikholeslami M, Ghasemi A, Li Z, Shafee A, Saleem S. Influence of CuO nanoparticles on heat transfer behavior of PCM in solidification process considering radiative source term. Int J Heat Mass Transf 2018;126:1252–64. https://doi.org/10.1016/j.ijheatmasstransfer.2018.05.116.

[8] Mahdi JM, Nsofor EC. Melting enhancement in triplex-tube latent thermal energy storage system using nanoparticles-fins combination. Int J Heat Mass Transf 2017;109:417–27. https://doi.org/10.1016/j.ijheatmasstransfer.2017.02.016.

[9] Agyenim F, Eames P, Smyth M. Heat transfer enhancement in medium temperature thermal energy storage system using a multitube heat transfer array. Renew Energy 2010;35:198–207. https://doi.org/10.1016/j.renene.2009.03.010.

[10] Liu S, Peng H, Hu Z, Ling X, Huang J. Solidification performance of a latent heat storage unit with innovative longitudinal triangular fins. Int J Heat Mass Transf 2019;138:667–76. https://doi.org/10.1016/j.ijheatmasstransfer.2019.04.121.

[11] Wu L, Zhang X, Liu X. Numerical analysis and improvement of the thermal performance in a latent heat thermal energy storage device with spiderweb-like fins. J Energy Storage 2020;32:101768. https://doi.org/10.1016/j.est.2020.101768.

[12] Huang Y, Sun Q, Yao F, Zhang C. Performance optimization of a finned shell-and-tube ice storage unit. Appl Therm Eng 2020;167:114788. https://doi.org/10.1016/j.applthermaleng.2019.114788.

[13] Patel JR, Rathod MK, Elavarasan RM, Said Z. Influence of longitudinal fin arrangement on the melting and solidification inside the triplex tube latent heat thermal storage system. J Energy Storage 2022;46:103778. https://doi.org/10.1016/j.est.2021.103778.

[14] Sheikholeslami M, Haq R-ul, Shafee A, Li Z. Heat transfer behavior of nanoparticle enhanced PCM solidification through an enclosure with V shaped fins. Int J Heat Mass Transf 2019;130:1322–42. https://doi.org/10.1016/j.ijheatmasstransfer.2018.11.020.

[15] Mahdi JM, Lohrasbi S, Ganji DD, Nsofor EC. Simultaneous energy storage and recovery in the triplex-tube heat exchanger with PCM, copper fins and Al2O3 nanoparticles. Energy Convers Manag 2019;180:949–61. https://doi.org/10.1016/j.enconman.2018.11.038.

[16] Hosseinzadeh K, Alizadeh M, Tavakoli MH, Ganji DD. Investigation of phase change material solidification process in a LHTESS in the presence of fins with variable thickness and hybrid nanoparticles. Appl Therm Eng 2019;152:706–17. https://doi.org/10.1016/j.applthermaleng.2019.02.111.

[17] Qin Y. Numerical modeling of energy storage unit during freezing of paraffin utilizing Al2O3 nanoparticles and Y-shape fin. J Energy Storage 2021;44:103452. https://doi.org/10.1016/j.est.2021.103452.

[18] Alizadeh M, Hosseinzadeh K, Shahavi MH, Ganji DD. Solidification acceleration in a triplex-tube latent heat thermal energy storage system using V-shaped fin and nano-enhanced phase change material. Appl Therm Eng 2019;163:114436. https://doi.org/10.1016/j.applthermaleng.2019.114436.

[19] Sarani I, Payan S, Nada SA, Payan A. Numerical investigation of an innovative discontinuous distribution of fins for solidification rate enhancement in PCM with and without nanoparticles. Appl Therm Eng 2020;176:115017. https://doi.org/10.1016/j.applthermaleng.2020.115017.

[20] Mahdi JM, Nsofor EC. Solidification of a PCM with nanoparticles in triplex-tube thermal energy storage system. Appl Therm Eng 2016;108:596–604. https://doi.org/10.1016/j.applthermaleng.2016.07.130.

[21] Elbahjaoui R, El Qarnia H. Transient behavior analysis of the melting of nanoparticle-enhanced phase change material inside a rectangular latent heat storage unit. Appl Therm Eng 2017;112:720–38. https://doi.org/10.1016/j.applthermaleng.2016.10.115.

[22] García-Valladares O. Numerical simulation of triple concentric-tube heat exchangers. Int J Therm Sci 2004;43:979–91. https://doi.org/10.1016/j.ijthermalsci.2004.02.006.

[23] Al-Abidi AA, Mat S, Sopian K, Sulaiman MY, Mohammad AT. Experimental study of melting and solidification of PCM in a triplex tube heat exchanger with fins. Energy Build 2014;68:33–41. https://doi.org/10.1016/j.enbuild.2013.09.007.

[24] Zhang J, Cao Z, Huang S, Huang X, Liang K, Yang Y, Zhang H, Tian M, Akrami M, Wen C. Improving the melting performance of phase change materials using novel fins and nanoparticles in tubular energy storage systems. Appl Energy 2022;322:119416. https://doi.org/10.1016/j.apenergy.2022.119416.

[25] Ma J, Xu H, Liu S, Peng H, Ling X. Numerical study on solidification behavior and exergy analysis of a latent heat storage unit with innovative circular superimposed longitudinal fins. Int J Heat Mass Transf 2021;169:120949. https://doi.org/10.1016/j.ijheatmasstransfer.2021.120949.

[26] Zonouzi SA, Dadvar A. Numerical investigation of using helical fins for the enhancement of the charging process of a latent heat thermal energy storage system. J Energy Storage 2022;49:104157. https://doi.org/10.1016/j.est.2022.104157.

[27] Shmueli H, Ziskind G, Letan R. Melting in a vertical cylindrical tube: numerical investigation and comparison with experiments. Int J Heat Mass Transf 2010;53:4082–91. https://doi.org/10.1016/j.ijheatmasstransfer.2010.05.028.

[28] Palmer B, Arshad A, Yang Y, Wen C. Energy storage performance improvement of phase change materials-based triplex-tube heat exchanger (TTHX) using liquid–solid interface-informed fin configurations. Appl Energy 2023;333:120576. https://doi.org/10.1016/j.apenergy.2022.120576.

[29] Yan P, Fan W, Yang Y, Ding H, Arshad A, Wen C. Performance enhancement of phase change materials in triplex-tube latent heat energy storage system using novel fin configurations. Appl Energy 2022;327:120064. https://doi.org/10.1016/j.apenergy.2022.120064.

[30] Han Y, Yang Y, Mallick T, Wen C. Nanoparticles to enhance melting performance of phase change materials for thermal energy storage. Nanomaterials 2022;12(11):1864. https://doi.org/10.3390/nano12111864.

[31] Vajjha RS, Das DK. Experimental determination of thermal conductivity of three nanofluids and development of new correlations. Int J Heat Mass Transf 2009;52:4675–82. https://doi.org/10.1016/j.ijheatmasstransfer.2009.06.027.

[32] Du Z, Liu G, Huang X, Xiao T, Yang X, He Y-L. Numerical studies on a fin-foam composite structure towards improving melting phase change. Int J Heat Mass Transf 2023;208:124076. https://doi.org/10.1016/j.ijheatmasstransfer.2023.124076.

[33] Li F, Huang X, Li Y, Lu L, Meng X, Yang X, Sundén B. Application and analysis of flip mechanism in the melting process of a triplex-tube latent heat energy storage unit. Energy Rep 2023;9:3989–4004. https://doi.org/10.1016/j.egyr.2023.03.037.

[34] Xiao T, Liu G, Guo J, Shu G, Lu L, Yang X. Effect of metal foam on improving solid–liquid phase change in a multi-channel thermal storage tank. Sustainable Energy Technol Assess 2022:53. https://doi.org/10.1016/j.seta.2022.102533.

[35] Liu G, Du Z, Xiao T, Guo J, Lu L, Yang X, Hooman K. Design and assessments on a hybrid pin fin-metal foam structure towards enhancing melting heat transfer: an experimental study. Int J Therm Sci 2022;182. https://doi.org/10.1016/j.ijthermalsci.2022.107809.

[36] Xiao T, Liu Z, Lu L, Han H, Huang X, Song X, Yang X, Meng X. LSTM-BP neural network analysis on solid-liquid phase change in a multi-channel thermal storage tank. Eng Anal Bound Elem 2023;146:226–40. https://doi.org/10.1016/j.enganabound.2022.10.014.

[37] Huang X, Li F, Xiao T, Guo J, Wang F, Gao X, Yang X, He Y-L. Investigation and optimization of solidification performance of a triplex-tube latent heat thermal energy storage system by rotational mechanism. Appl Energy 2023;331. https://doi.org/10.1016/j.apenergy.2022.120435.

[38] Leonard BP. A stable and accurate convective modelling procedure based on quadratic upstream interpolation. Comput Methods Appl Mech Eng 1979;19:59–98. https://doi.org/10.1016/0045-7825(79)90034-3.